Supporting Information

Solar-driven Reduction of Aqueous Protons Coupled to Selective Alcohol Oxidation with a Carbon Nitride - Molecular Ni Catalyst System

Hatice Kasap,[1] Christine A. Caputo,[1] Benjamin C. M. Martindale,[1] Robert Godin,[2] Vincent Wing-hei Lau,[3,4] Bettina V. Lotsch,[3,4,*] James R. Durrant,[2,*] Erwin Reisner[1,*]

[1]Christian Doppler Laboratory for Sustainable SynGas Chemistry, Department of Chemistry, University of Cambridge, Lensfield Road, Cambridge CB2 1EW, UK

[2]Department of Chemistry, Imperial College London, Exhibition Road, London SW7 2AZ, UK

[3]Max Planck Institute for Solid State Research, Heisenbergstrasse 1, 70569 Stuttgart, Germany

[4]Department of Chemistry, Ludwig-Maximilians-Universität München, Butenandtstrasse 5–13 (Haus D), 81377 München, Germany

Corresponding authors:

reisner@ch.cam.ac.uk

j.durrant@imperial.ac.uk

b.lotsch@fkf.mpg.de

Contents

Analysis of Transient Absorption Spectroscopy Data

Decays could be fit to a power law of the form $y = y_0 + |t - t_0|^{-b}$ (Figure S20). t_0 represents the time offset between the trigger signal and the arrival of the excitation pulse to the sample, while y_0 is the absorbance offset at infinite times. The parameters b was ca. 0.35 and t_0 was typically 1 x 10^{-7} s. No trends with respect to the concentration of 4-MBA or **NiP** were observed.

In order to quantify the concentration of long-lived species, we used the amplitude at 3 μs to estimate the initial population of excited species, and the amplitude at 100 ms for the population of long-lived species. The yield of the long-lived species is then calculated as:

$$\Phi_{long-lived} = \frac{A_{t=100ms}}{A_{t=3\mu s}} \quad \text{(S1)}$$

The calculated yields are shown in Figure S22. As mentioned in the main text, the amplitude at 3 μs will underestimate the excited state species concentration immediately after the excitation pulse. As a result, the yields calculated from equation S1 are overestimated. Without data spanning femtoseconds to nanoseconds under similar excitation conditions, we are not able to quantify the total photogenerated excited species population. Despite the issues identified, the data clearly indicate that 4-MBA affect the transient absorption signal in the microsecond timescale while reaction with **NiP** occurs on timescales longer than 2 s.

Assuming dynamic quenching, we can estimate the bimolecular rate constant of hole transfer from $^{NCN}\mathbf{CN_x}$* to 4-MBA (k_{rxn}) by first writing the expression for the yield for competitive kinetics:

$$\Phi_{long-lived} = \frac{k_{form}}{k_{1/2} + k_{form}} \quad \text{(S2)}$$

$$where\ k_{form} = k_0 + k_{rxn}[4-MBA]$$

$k_{1/2}$ is the inverse of the characteristic lifetime ($\tau_{½}$) of the decay of $^{NCN}\mathbf{CN_x}$ without scavengers. We then rearrange equation S2 to calculate the rate of formation (k_{form}):

$$k_{form} = -\frac{\Phi_{long-lived} k_{1/2}}{\Phi_{long-lived} - 1} \quad \text{(S3)}$$

Finally, a linear fit of the plot k_{form} vs. [4-MBA] yields k_{rxn} as the slope.

Table S1. Solar light driven simultaneous H_2 and aldehyde production with **NiP** and ^{NCN}**CN$_x$**. Experiments were performed using ^{NCN}**CN$_x$** (5 mg) in aqueous potassium phosphate buffer (KP_i) at pH 4.5 (0.02 M) containing 4-methyl benzyl alcohol (4-MBA) and **NiP** as a hydrogen evolution catalyst. All the photocatalytic experiments were carried out under N_2 containing 2% CH_4, the vials were irradiated with simulated solar light (AM 1.5G) in water-jacketed rack at 25°C. Total solvent volume was 3 mL with a headspace volume of 4.74 ml. Entry **9** displays the optimized conditions. All the experiments showed 100% selectivity towards aldehyde formation and no carboxylic acid was detected.

Entry	NiP / nmol	Alcohol/ μmol	pH of the solution	Aldehyde ± σ / μmol (after 24 h)	Alcohol Conversion ± σ / (%)	H_2 ± σ / μmol (after 24 h)	TON (24 h) ± σ / mol H_2 NiP^{-1}	Activity/ μmol H_2 (g CN_x)$^{-1}h^{-1}$ (after 1h)	TOF ± σ / h^{-1} (after 1h)
pH dependence									
1	50	30	3	14.63 ± 2.35	48.77 ± 7.83	13.13 ± 1.31	262.63 ± 26.26	293.36 ± 29.34	29.34 ± 2.93
2	50	30	4.5	19.80 ± 19.8	66.0 ± 6.60	21.27 ± 2.13	425.38 ± 42.54	311.18 ± 31.12	31.12 ± 3.11
3	50	30	6	16.25 ± 1.62	54.16 ± 5.42	14.80 ± 1.48	296.02 ± 29.60	232.70 ± 23.27	23.27 ± 2.33
[Alcohol] dependence									
4	50	15	4.5	11.93 ± 1.19	79.51 ± 7.95	13.46 ± 1.35	269.17 ± 26.92	266.89 ± 26.69	26.69 ± 2.67
5	50	30	4.5	19.80 ± 1.98	66.0 ± 6.60	21.27 ± 2.13	425.38 ± 42.54	311.18 ± 31.12	31.12 ± 3.11
6	50	60	4.5	16.54 ± 1.71	27.57 ± 2.86	15.46 ± 1.55	309.13 ± 30.91	240.59 ± 24.06	24.06 ± 2.41
[NiP] dependence									
7	10	30	4.5	8.60 ± 0.86	28.67 ± 2.87	2.48 ± 0.46	247.72 ± 46.10	86.83 ± 9.70	43.42 ± 4.85
8	25	30	4.5	11.10 ± 2.46	37.00 ± 8.19	5.22 ± 1.21	208.95 ± 48.37	158.51 ± 15.85	31.70 ± 3.17
9	50	30	4.5	19.80 ± 1.98	66.0 ± 6.60	21.27 ± 2.13	425.38 ± 42.54	311.18 ± 31.12	31.12 ± 3.11
10	100	30	4.5	24.60 ± 2.95	82.00 ± 9.85	24.97 ± 2.50	249.72 ± 24.97	409.80 ± 40.98	20.49 ± 2.05

Table S2. Time dependent solar light driven H_2 and aldehyde production in the presence of $^{NCN}CN_x$ (5 mg), 4-MBA (30 μmol) and **NiP** (50 nmol) in aqueous KP_i (0.02 M, pH 4.5, 3 mL) with 1 sun irradiation (AM 1.5G) in water-jacketed rack at 25°C. All the experiments showed 100% selectivity towards aldehyde formation and no carboxylic acid was detected.

Entry	Time / h	Aldehyde ± σ / μmol	Alcohol Conversion ± σ / (%)	H_2 ± σ / μmol	TON ± σ / mol H_2 NiP^{-1}
11	1	2.37 ± 0.47	7.90 ± 1.56	1.64 ± 0.16	32.88 ± 3.23
12	2	3.55 ± 0.84	11.84 ± 2.79	3.74 ± 0.37	74.83 ± 7.48
13	3	5.33 ± 0.53	17.78 ± 1.78	5.23 ± 0.52	104.59 ± 10.46
14	4	6.55 ± 0.66	21.84 ± 2.18	5.92 ± 0.59	118.30 ± 11.83
15	5	6.65 ± 0.66	22.16 ± 2.22	8.04 ± 0.80	160.72 ± 16.07
16	6	8.27 ± 1.39	27.57 ± 4.64	10.28 ± 1.03	205.66 ± 20.57
17	12	11.47 ± 1.51	38.57 ± 4.64	12.37 ± 1.24	247.40 ± 24.74
18	24	19.80 ± 1.98	66.0 ± 6.60	21.27 ± 2.13	425.38 ± 42.54

Table S3. Photocatalytic H_2 and aldehyde production in the presence $^{NCN}\mathbf{CN_x}$ (5 mg), 4-MBA (30 μmol) and **NiP** (50 nmol) in aqueous KP_i (0.02 M, pH 4.5, 3 mL) under visible-light-only (λ > 400 nm) irradiation. Control experiments were also performed in the absence of $^{NCN}\mathbf{CN_x}$, **NiP**, 4-MBA and in dark. Different para substituted benzyl alcohol (BA) derivatives (30 μmol) were tested in the presence $^{NCN}\mathbf{CN_x}$ (5 mg) and **NiP** (50 nmol) in aqueous KP_i (0.02 M, pH 4.5, 3 mL) under 1 sun irradiation (AM 1.5G). All the experiments showed 100% selectivity towards aldehyde formation and no carboxylic acid was detected unless specified otherwise.

Entry	NiP / nmol	Alcohol	Alcohol/ μmol	Aldehyde ± σ / μmol (after 24 h)	Alcohol Conversion (%)	Selectivity ± σ / (%)	H_2 ± σ / μmol (after 24 h)	TON (24 h) ± σ / mol H_2 NiP^{-1}	Activity/ μmol H_2 $(g\ CN_x)^{-1}h^{-1}$ (after 1h)	TOF ± σ / h^{-1} (after 1h)
Visible Light only Irradiation (λ > 400 nm)										
19	50	4-MBA	30	10.02 ± 2.08	33.67 ± 6.50	100	10.31 ± 1.20	206.25 ± 24.07	122.93 ± 12.29	12.29 ± 1.23
Control Experiments										
20	0	4-MBA	30	7.30 ± 0.73	24.33 ± 2.43	100	0.33 ± 0.03	−	3.37 ± 3.37	−
21	50	0	−	−	−	−	0.11 ± 0.02	2.10 ± 0.30	16.04 ± 3.05	1.60 ± 0.31
22	50, No $^{NCN}CN_x$	4-MBA	30	0	0	−	0	0	−	−
23	50, dark	4-MBA	30	0	0	−	0	0	0	0
Alcohol Dependence										
24	50	BA	30	13.70 ± 2.70	45.67 ± 9.02	100	21.47 ± 2.15	429.55 ± 42.96	289.62 ± 39.48	28.96 ± 3.95
25	50	4-OMeBA	30	13.73 ± 1.37	45.78 ± 4.58	100	9.84 ± 0.98	196.70 ± 19.67	233.33 ± 23.33	23.33 ± 2.33
26	50	4-ClBA	30	13.4 ± 2.11	44.67 ± 7.02	100	14.06 ± 2.98	281.23 ± 59.60	254.09 ± 25.41	25.41 ± 2.51
27	50	4-CF_3BA	30	1.83 ± 0.61	6.09 ± 2.03	100	5.15 ± 0.55	103.09 ± 11.04	99.60 ± 9.96	9.96 ± 1.00
28	50	4-^{t}BuBA	30	7.84 ± 1.41	40.83 ± 9.00	64.33 ± 3.21*	9.90 ± 0.99	198.07 ± 19.80	823.24 ± 82.32	82.32 ± 8.23
29	50	MeOH	30	0	0	−	0	0	0	0

*These experiments resulted in 41% alcohol oxidation with 64% selectivity towards 4-*tert*-Butylbenzaldehyde and 36% to 4-*tert*-Butylbenzoic acid formation.

Table S4. Solar light driven H_2 and aldehyde production in the presence of $^{NCN}CN_x$ (5 mg), 4-MBA (30 μmol) and **NiP** (50 nmol) in aqueous sodium acetate buffer, and KP_i (pH 4.5, 3 mL) at different concentrations under 1 sun irradiation (AM 1.5G). Sacrificial conditions were also tested in EDTA (0.1 M, pH 4.5, 3 mL), TEOA (0.1 M, pH 4.5, 3 mL) and in KP_i (0.02 M, pH 4.5, 3 mL) under air. All the experiments showed 100% selectivity towards aldehyde formation and no carboxylic acid was detected unless specified otherwise.

Entry	NiP / nmol	Alcohol	Alcohol/ μmol	Solution	Solution Concentration	Aldehyde ± σ / μmol (after 24 h)	Alcohol Conversion ± σ / (%)	H_2 ± σ / μmol (after 24 h)	TON (24 h) ± σ / mol H_2 NiP^{-1}	Activity/ μmol H_2 $(g\ CN_x)^{-1}\ h^{-1}$ (after 1h)	TOF ± σ / h^{-1} (after 1h)
Solution dependence											
30	50	4-MBA	30	CH_3COONa	0.1 M	12.03 ± 1.20	40.11 ± 4.01	9.69 ± 0.97	193.74 ± 19.37	360.02 ± 36.00	36.00 ± 3.60
31	50	4-MBA	30	KP_i	0.1 M	24.90 ± 2.49	83.0 ± 8.30	20.44 ± 2.04	408.76 ± 40.88	762.70 ± 76.27	76.27 ± 7.63
32	50	4-MBA	30	KP_i	0.5 M	18.13 ± 1.81	60.44 ± 6.04	18.62 ± 1.86	372.39 ± 37.24	1114.21 ± 111.42	111.42 ± 11.14
33	50	4-MBA	30	KP_i + KCl	0.02 M + 0.08 M	20.27 ± 3.77	67.56 ± 12.58	23.34 ± 2.33	466.78 ± 46.68	539.28 ± 59.12	53.93 ± 5.91
34	50	4-MBA	30	KP_i + K_2SO_4	0.02 M + 0.08 M	20.00 ± 2.00	66.67 ± 6.67	20.97 ± 2.10	419.45 ± 41.95	492.04 ± 49.20	49.20 ± 4.92
Sacrificial Conditions											
35	50	0	−	EDTA	0.1 M	−	−	21.21 ± 2.12	424.18 ± 42.42	532.32 ± 53.22	52.23 ± 5.23
36	0	4-MBA	30	KP_i, under air	−	6.04 ± 2.09	100†	−	−	−	−
37	0, dark	4-MBA	30	KP_i, under air	−	0	0	−	−	−	−

†These experiments resulted in 100% alcohol conversion with 70% selectivity towards 4-methyl benzoic acid, 20% 4-methyl benzaldehyde and 10% to further oxidation products (benzene-1, 4-dicarbaldehyde and 4-formylbenzoic acid) formation.

Table S5. Photocatalytic H_2 and aldehyde production with ^{H2N}**CN$_x$** (5 mg), 4-MBA (30 μmol) and **NiP** (50 nmol) in KP_i (0.02 M, pH 4.5, 3 mL) were conducted under 1 sun irradiation (AM 1.5G, 25°C). Photocatalytic experiments in the presence of ^{NCN}**CN$_x$** (5 mg) or ^{H2N}**CN$_x$** (5 mg), 4-MBA (30 μmol) and H_2PtCl_6 (10 μL, 8 wt. %) in KP_i (0.02 M, pH 4.5, 3 mL) were also carried out. A control experiment in EDTA (0.1 M, pH 4.5, 3 mL) solution with 4-methyl benzaldehyde (4-MBAd), ^{NCN}**CN$_x$** (5 mg) and H_2PtCl_6 was also tested. All the experiments showed 100% selectivity towards aldehyde formation and no carboxylic acid was detected unless specified otherwise.

Entry	Catalyst used	CN_x type	Substrate	Solution	Aldehyde ± σ / μmol (after 24 h)	Substrate Conversion ± σ / (%)	H_2 ± σ / μmol (after 24 h)	TON (24 h) ± σ / mol H_2 NiP^{-1}	Activity/ μmol H_2 (g $CN_x)^{-1}$ h^{-1} (after 1h)	TOF ± σ / h^{-1} (after 1h)
Irradiate for 4 h										
38	NiP	$^{H2N}CN_x$	4-MBA	KP_i	1.44 ± 0.71	4.80 ± 2.36	2.02 ± 0.20	40.31 ± 4.03	125.05 ± 12.50	12.50 ± 1.25
39	Pt[#]	$^{H2N}CN_x$	4-MBA	KP_i	1.28 ± 0.55	4.26 ± 1.85	0	0	0	0
40	Pt[#]	$^{NCN}CN_x$	4-MBA	KP_i	1.79 ± 1.21	5.98 ± 4.05	1.56 ± 0.16	0.80 ± 0.08	170.68 ± 18.97	0.44 ± 0.05
Irradiate for 24 h										
41	NiP	$^{H2N}CN_x$	4-MBA	KP_i	1.44 ± 0.71	4.80 ± 2.36	2.49 ± 0.71	49.79 ± 14.18	117.30 ± 11.73	11.73 ± 1.17
42	Pt[#]	$^{NCN}CN_x$	4-MBA	KP_i	11.99 ± 2.29	41.1 ± 7.85[‡]	14.22 ± 1.42	7.29 ± 0.73	138.43 ± 13.08	0.35 ± 0.03
43	Pt[#]	$^{NCN}CN_x$	4-MBAd	EDTA	5.42 ± 0.54	18.07 ± 1.81**	3.50 ± 0.44	1.79 ± 0.23	9.46 ± 4.88	0.02 ± 0.01

[#]These experiments were conducted in the presence of 10 μL of 8 wt% aqueous solution of H_2PtCl_6 corresponding for 8 wt% Pt loading (in the absence of **NiP**).

[‡]These experiments resulted in 41% alcohol oxidation with 97:3% selectivity towards 4-methyl benzaldehyde and 4-methylbenzoic acid formation respectively.

** These experiments resulted in 18% 4-methylbenzoic acid formation.

Table S6. Photocatalytic H_2 and aldehyde production in the presence of $^{NCN}CN_x$ (5 mg), 4-MBA (30 μmol) and **NiP** (50 nmol) in KP_i (0.02 M, pH 4.5, 3 mL) with the addition of neutral density filters (50% and 80% absorbance of the incident light) were conducted. All the experiments showed 100% selectivity towards aldehyde formation and no carboxylic acid was detected.

Entry	Aldehyde ± σ / μmol (after 1 h)	Alcohol Conversion ± σ / (%)	Selectivity ± σ / (%)	H_2 ± σ / μmol (after 1 h)	Activity/ μmol H_2 (g CN_x)$^{-1}$ h^{-1} (after 1h)	TOF ± σ / h^{-1} (after 1h)
No neutral density filter						
44	2.29 ± 0.23	7.64 ± 0.76	100	1.49 ± 0.15	297.73 ± 18.29	29.77 ± 1.83
50 % neutral density filter						
45	1.37 ± 0.16	4.27 ± 0.43	100	0.95 ± 0.10	190.01 ± 12.35	19.00 ± 1.90
80 % neutral density filter						
46	0.88 ± 0.09	2.94 ± 0.29	100	0.54 ± 0.05	108.30 ± 1.87	10.83 ± 1.08

Table S7. Long-term photocatalytic H_2 and Aldehyde production in the presence of $^{NCN}CN_x$ (5 mg), 4-MBA (30 μmol) and **NiP** (50 nmol) in KP_i (0.02 M, pH 4.5, 3 mL) under 1 sun irradiation (AM 1.5G, 25°C). After 25 h of irradiation, fresh **NiP** (50 nmol), fresh 4-MBA (30 μmol), and both **NiP** (50 nmol) and 4-MBA (30 μmol) were added to photoreactors to test the system re-activation, and placed back into solar light simulator for monitoring over 25 more h (Total irradiation time of 50 h). All the experiments showed 100% selectivity towards aldehyde formation and no carboxylic acid was detected.

Entry	NiP / nmol	Alcohol/ μmol	Aldehyde ± σ / μmol	Alcohol Conversion ± σ / (%)	H_2 ± σ / μmol	Activity/ μmol H_2 (g CN_x)$^{-1}$ h^{-1} (after 1h)	TOF ± σ / h^{-1} (after 1h)
Re-activation by NiP addition							
47	50+50	30	25.04 ± 2.90	83.47 ± 9.66	26.96 ± 2.70	244.59 ± 24.46	24.46 ± 2.45
Re-activation by 4-MBA addition							
48	50	30+30	13.47 ± 2.40	22.44 ± 3.99	16.97 ± 1.70	230.21 ± 12.92	23.02 ± 2.30
Re-activation by NiP and 4-MBA addition							
49	50+50	30+30	21.13 ± 2.21	35.21 ± 3.68	28.29 ± 2.83	227.86 ± 6.45	22.79 ± 2.28

Table S8. Two photoreactors were prepared with ^{NCN}**CN$_x$** (5 mg) and 4-MBA (30 μmol) in the absence of **NiP** in an aqueous KP_i solution (0.02 M, pH 4.5, 3 mL) and irradiated for 4 h under 1 sun (AM 1.5G, 25°C). The vials were then taken into the dark, **NiP** (50 nmol) was added to one of them and the H_2 production was monitored for both of the vials over the next 20 h.

Entry	NiP / nmol	Aldehyde ± σ / μmol	Alcohol Conversion ± σ / (%)	H_2 ± σ / μmol	TON (24 h) ± σ / mol H_2 NiP^{-1}	Activity/ μmol H_2 (g CN_x)$^{-1}$ h^{-1} (after 1h)	TOF ± σ / h^{-1} (after 1h)
Irradiate for 4h and move to dark							
50	0	1.56 ± 0.40	5.18 ± 1.34	0.26 ± 0.03	−	9.34 ± 0.09	−
Irradiate for 4h, move to dark and add NiP							
51	50	1.97 ± 0.65	6.50 ± 2.17	1.24 ± 0.12	24.89 ± 2.49	11.71 ± 1.17	1.17 ± 0.12

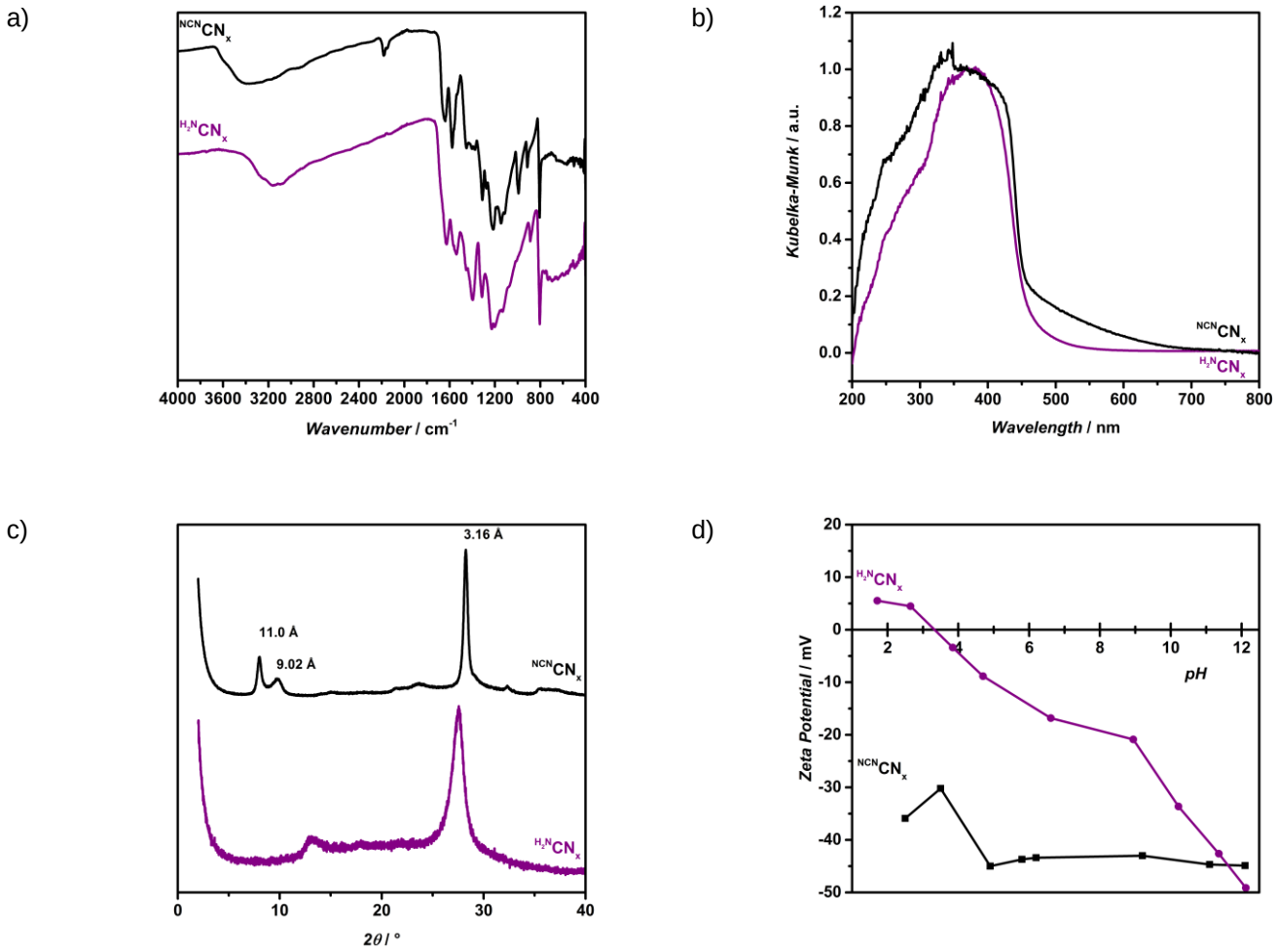

Figure S1. a) Fourier transform infrared spectroscopy (FTIR) spectra of $^{H2N}\mathbf{CN_x}$ and $^{NCN}\mathbf{CN_x}$. Both $^{H2N}\mathbf{CN_x}$ and $^{NCN}\mathbf{CN_x}$ showed characteristic heptazine core IR vibration at 804 cm^{-1} and bridging secondary amine –C–N bending vibrations at 1311 and 1221 cm^{-1}, confirming the polymeric nature of the materials. The appearance of the C≡N stretch at 2177 cm^{-1} in the IR spectrum of $^{NCN}\mathbf{CN_x}$ confirmed the presence of cyanamide group. b) Diffuse reflectance UV-vis spectra of $^{H2N}\mathbf{CN_x}$ and $^{NCN}\mathbf{CN_x}$. c) X-ray diffraction (XRD) patterns of $^{H2N}\mathbf{CN_x}$ and $^{NCN}\mathbf{CN_x}$. d) Zeta potential measurement for $^{H2N}\mathbf{CN_x}$ and $^{NCN}\mathbf{CN_x}$. Zeta potential of $^{NCN}\mathbf{CN_x}$ is -44 eV across all pH where the material is stable (pH > 4), which is attributed to the anionic cyanamide group on the surface. At pH below 4, the material lost its yellow color and turned white, indicative of cyanamide hydrolysis.[1]

a) b)

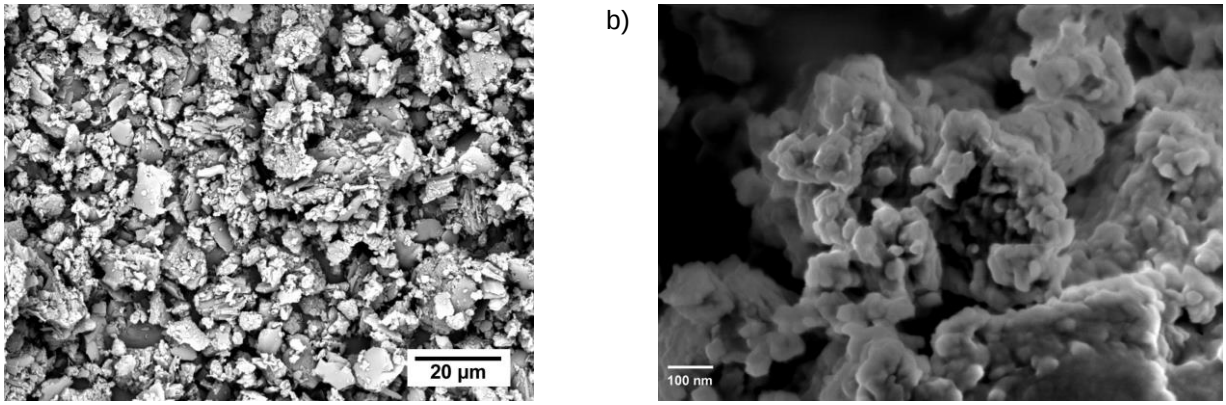

Figure S2. Scanning electron microscopy (SEM) image of a) $^{H2N}\mathbf{CN_x}$ and b) $^{NCN}\mathbf{CN_x}$.[1]

a) b)

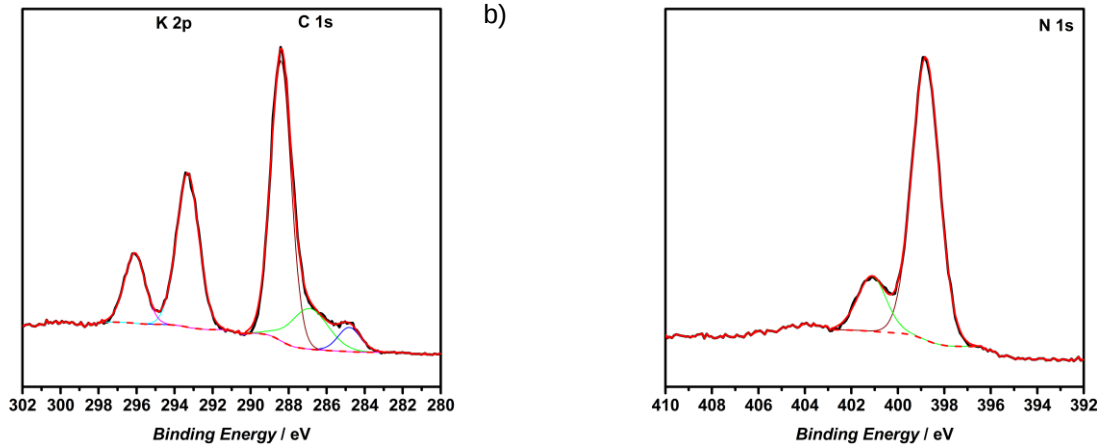

Figure S3. X-ray photoelectron spectra (XPS) of $^{NCN}\mathbf{CN_x}$ in the regions of a) K_{2p} and C_{1s} and b) N_{1s}. The heptazine core was identified by the presence of sp^2 carbon, 288.4 eV, and nitrogen, 398.8 eV, signals. The polymeric nature of the material was confirmed by the appearance of an XPS signal at 401.1 eV corresponding for the bridging secondary amine groups.[2]

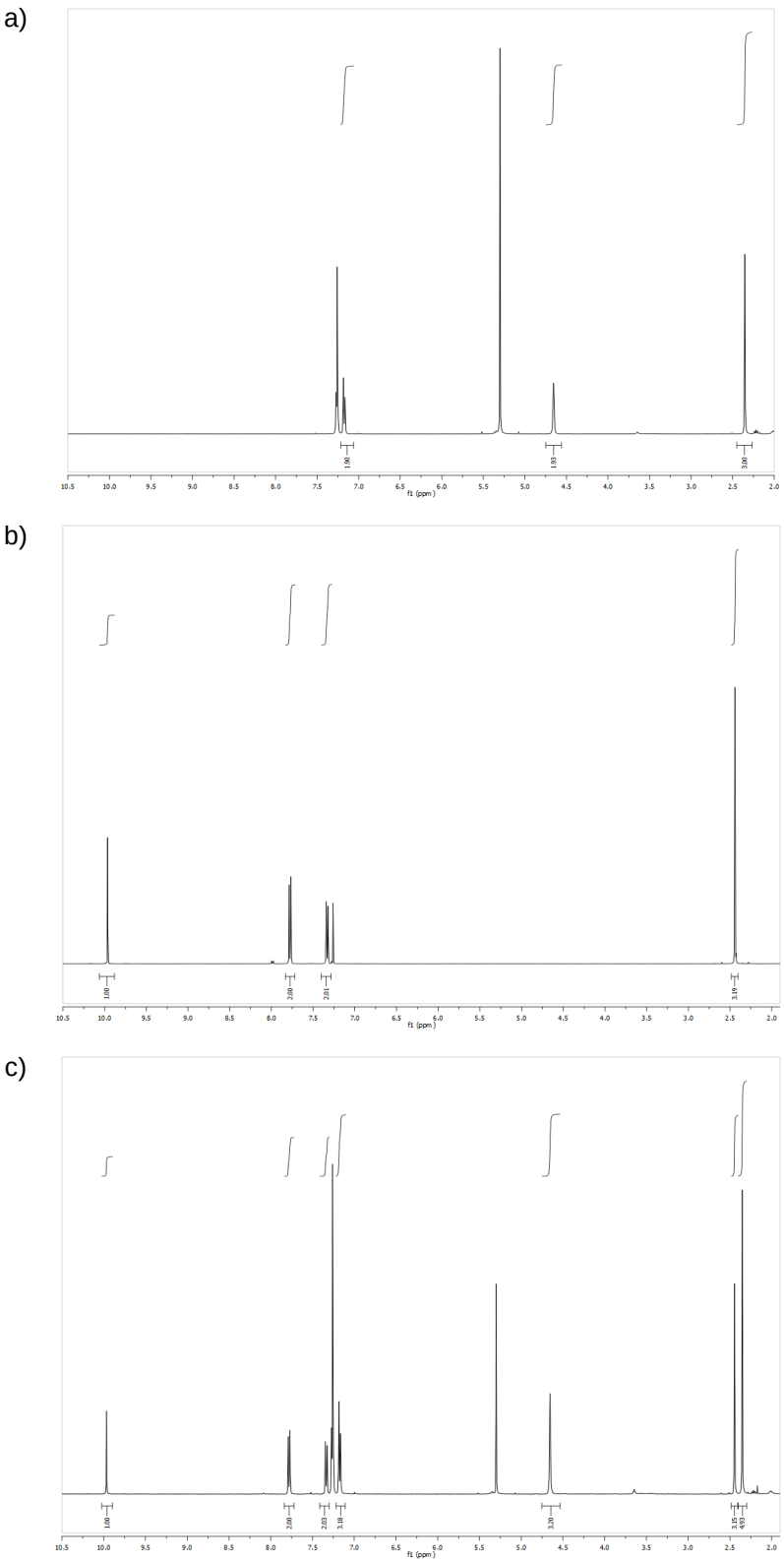

Figure S4. a) ^{1}H NMR spectra of 4-MBA, b) ^{1}H NMR spectra of 4-MBAd, c) a representative ^{1}H NMR spectra of the residue extracted after 24 h of irradiation in $CDCl_3$.

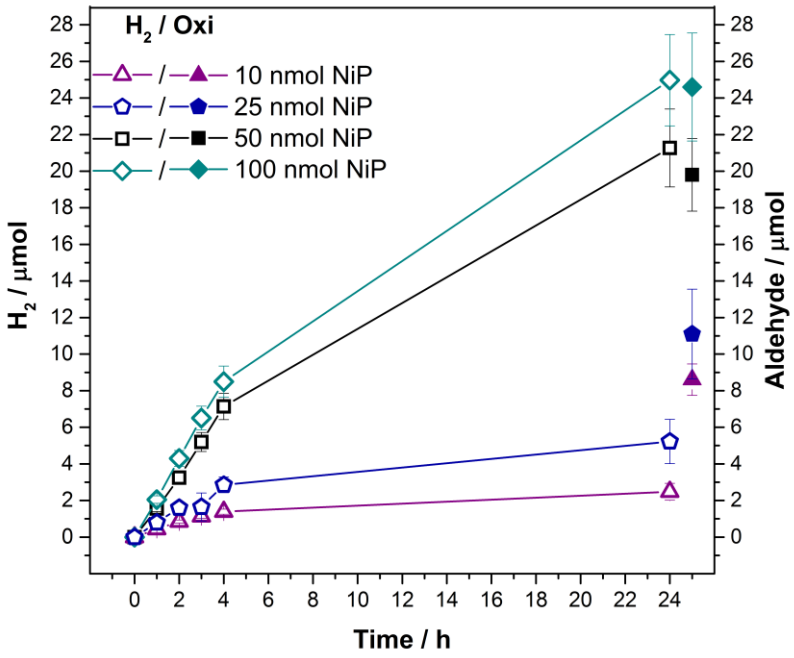

Figure S5. Photocatalytic H_2 and aldehyde production in an aqueous KP_i solution (0.02 M, pH 4.5, 3 mL) with $^{NCN}\mathbf{CN_x}$ (5 mg), 4-MBA (30 µmol) and different amount of **NiP** (1 sun irradiation, 100mW cm^{-2}, AM 1.5G, 25°C).

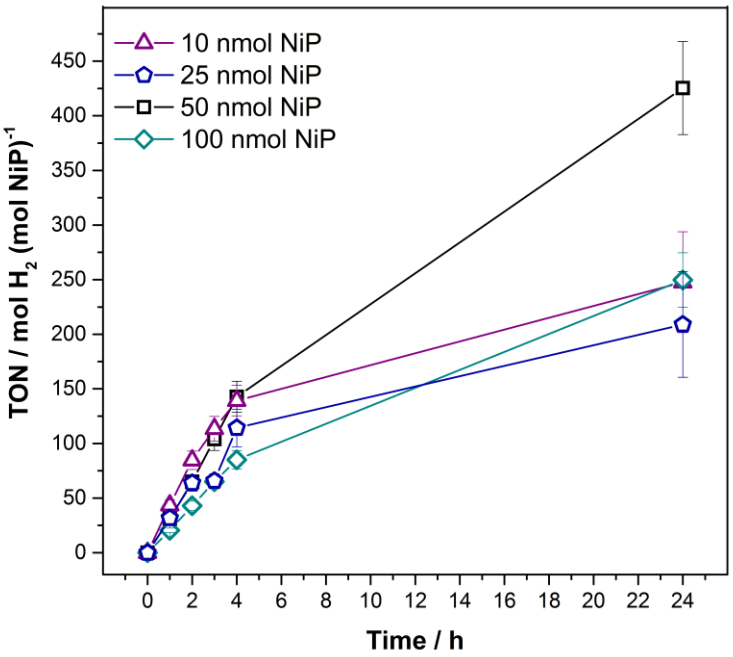

Figure S6. Photocatalytic TON_{NiP} in an aqueous KP_i solution (0.02 M, pH 4.5, 3 mL) with $^{NCN}\mathbf{CN_x}$ (5 mg), 4-MBA (30 µmol) and different amount of **NiP** (1 sun irradiation, 100mW cm^{-2}, AM 1.5G, 25°C).

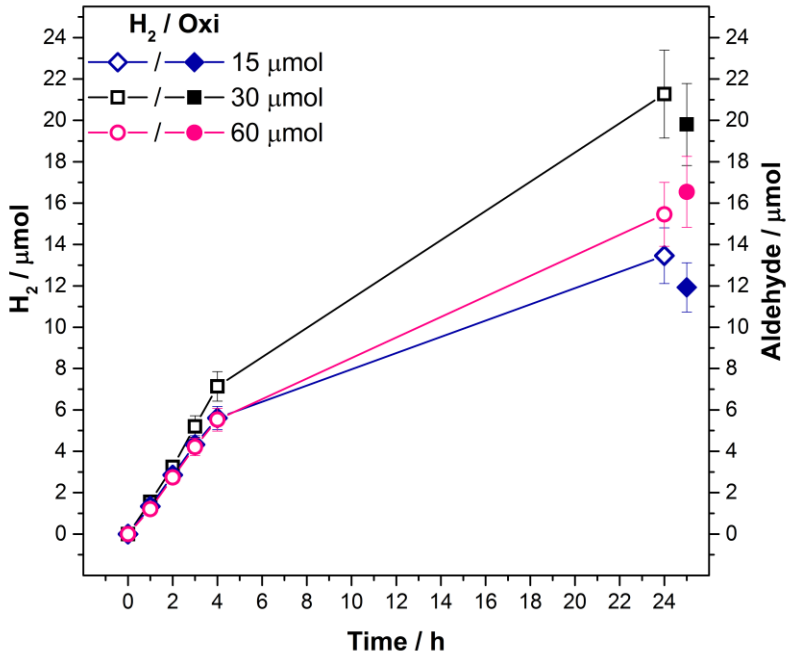

Figure S7. Photocatalytic H_2 and aldehyde production in the presence of $^{NCN}CN_x$ (5 mg) and **NiP** (50 nmol) with a varying amount of 4-MBA in an aqueous KP_i (0.02 M, pH 4.5, 3 mL) under 1 sun irradiation (100 mW cm^{-2}, AM 1.5G, 25°C).

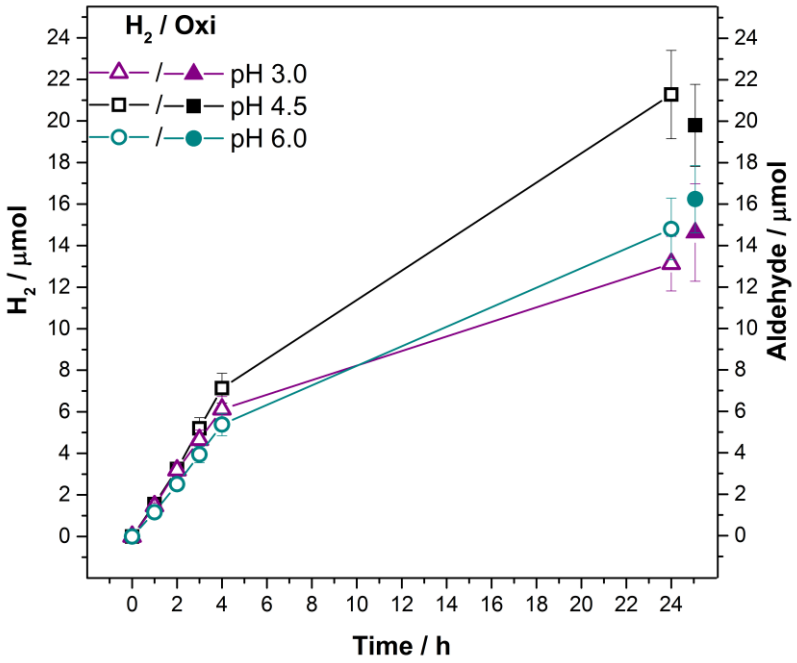

Figure S8. Photocatalytic H_2 and aldehyde production in the presence of $^{NCN}CN_x$ (5 mg), 4-MBA (30 µmol) with **NiP** (50 nmol) in an aqueous KP_i solution at various pH values (0.02 M, 3 mL) under 1 sun irradiation (100 mW cm^{-2}, AM 1.5G, 25°C).

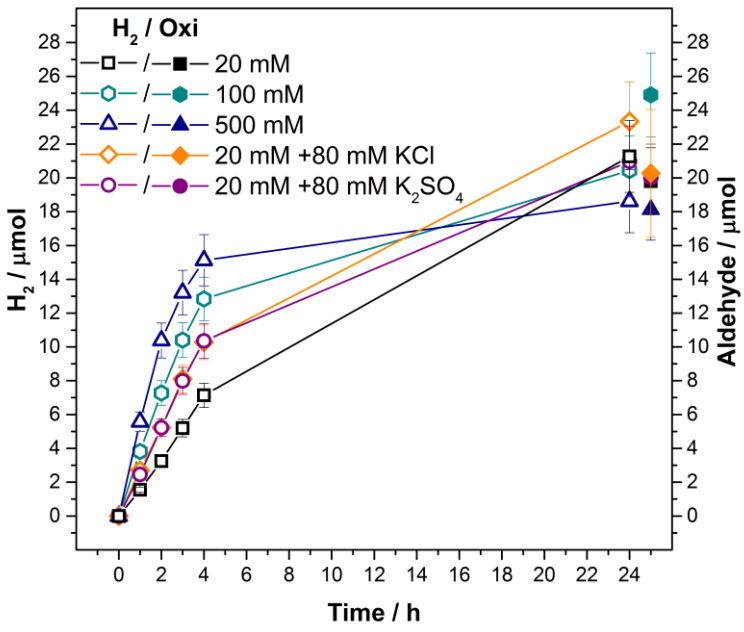

Figure S9. Photocatalytic H_2 and aldehyde production in the presence of ^{NCN}**CN$_x$** (5 mg), 4-MBA (30 µmol) and **NiP** (50 nmol) with varying the aqueous KP_i concentrations (pH 4.5, 3 mL) under 1 sun irradiation (100 mW cm^{-2}, AM 1.5G, 25 °C).

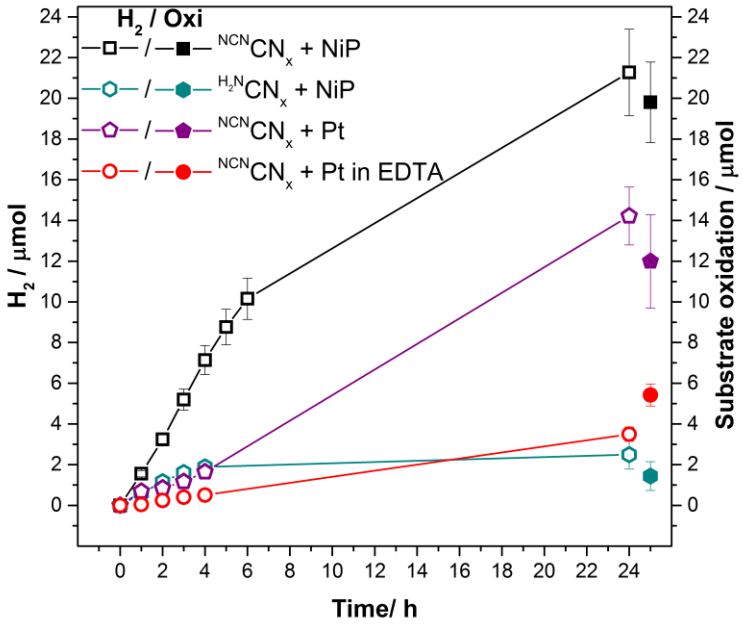

Figure S10. Photocatalytic H_2 and aldehyde production with ^{NCN}**CN$_x$** or ^{H2N}**CN$_x$** (5 mg), in the presence of 4-MBA (30 µmol) and **NiP** (50 nmol) in KP_i (0.02 M, pH 4.5, 3 mL) were conducted under 1 sun irradiation (AM 1.5G, 25°C). Photocatalytic experiments in the presence of ^{NCN}**CN$_x$**, 4-MBA (30 µmol) and H_2PtCl_6 (10 µL, 8 wt. %) in KP_i (0.02 M, pH 4.5, 3 mL) was also carried out. A control experiment in sacrificial EDTA solution (0.1 M, pH 4.5, 3 mL), ^{NCN}**CN$_x$** (5 mg), Pt (10 µL, 8 wt. %) and 4-MBAd (30 µmol) in the absence of **NiP** was carried out, to verify that Pt is only catalytically involved in proton reduction.

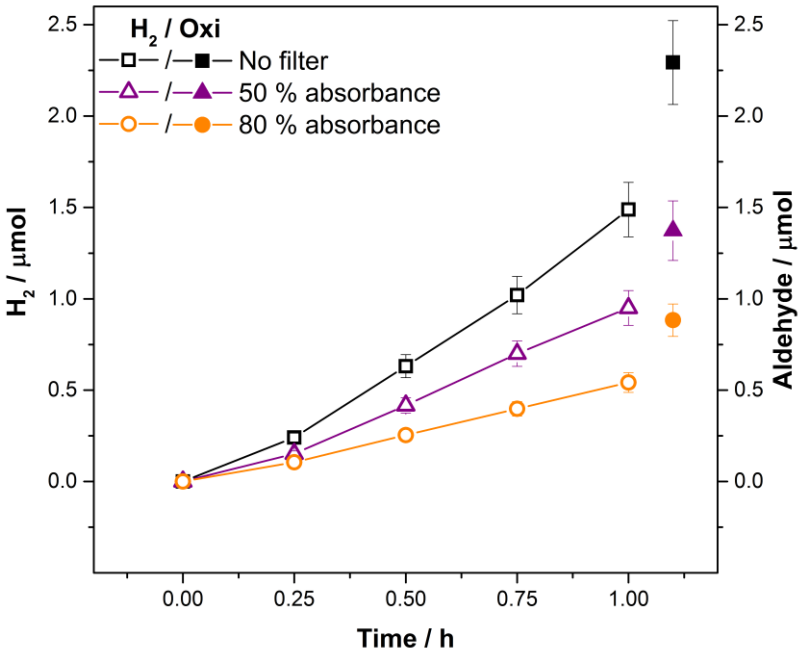

Figure S11. Photocatalytic H_2 and aldehyde production in the presence of $^{NCN}CN_x$ (5 mg), 4-MBA (30 µmol) and **NiP** (50 nmol) in an aqueous KP_i solution (0.02 M, pH 4.5, 3 mL) under 1 sun irradiation (AM 1.5G, 25°C), followed by the addition of neutral filter density filters that absorbs 50% and 80% of the incident light.

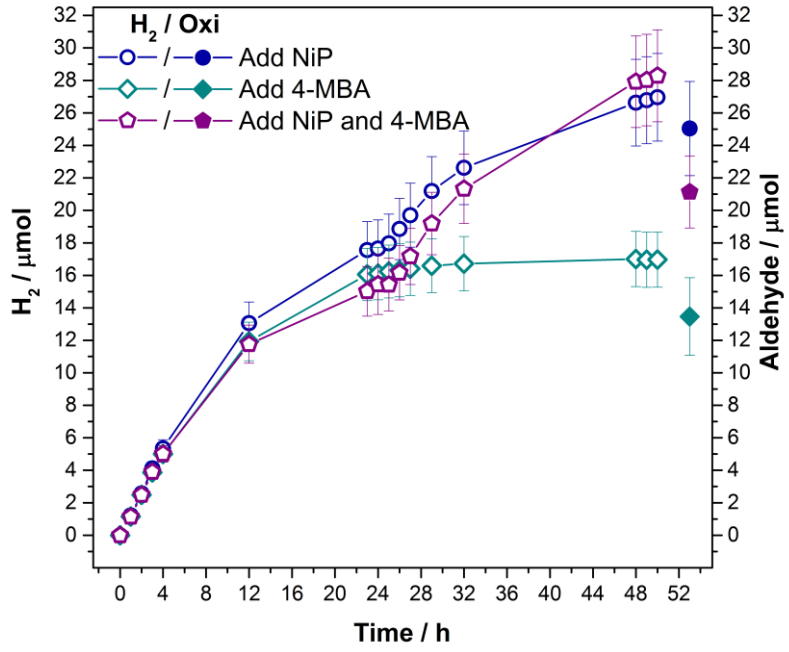

Figure S12. Long-term photocatalytic H_2 and aldehyde production in the presence of $^{NCN}CN_x$ (5 mg), 4-MBA (30 µmol) and **NiP** (50 nmol) in an aqueous KP_i (0.02 M, pH 4.5, 3mL) under 1 sun irradiation (AM 1.5G, 25°C). After 25 h of irradiation, **NiP** (50 nmol), 4-MBA (30 µmol), and both **NiP** (50 nmol) and 4-MBA (30 µmol) were added to photoreactors to test the system re-activation over the next 25 h of irradiation.

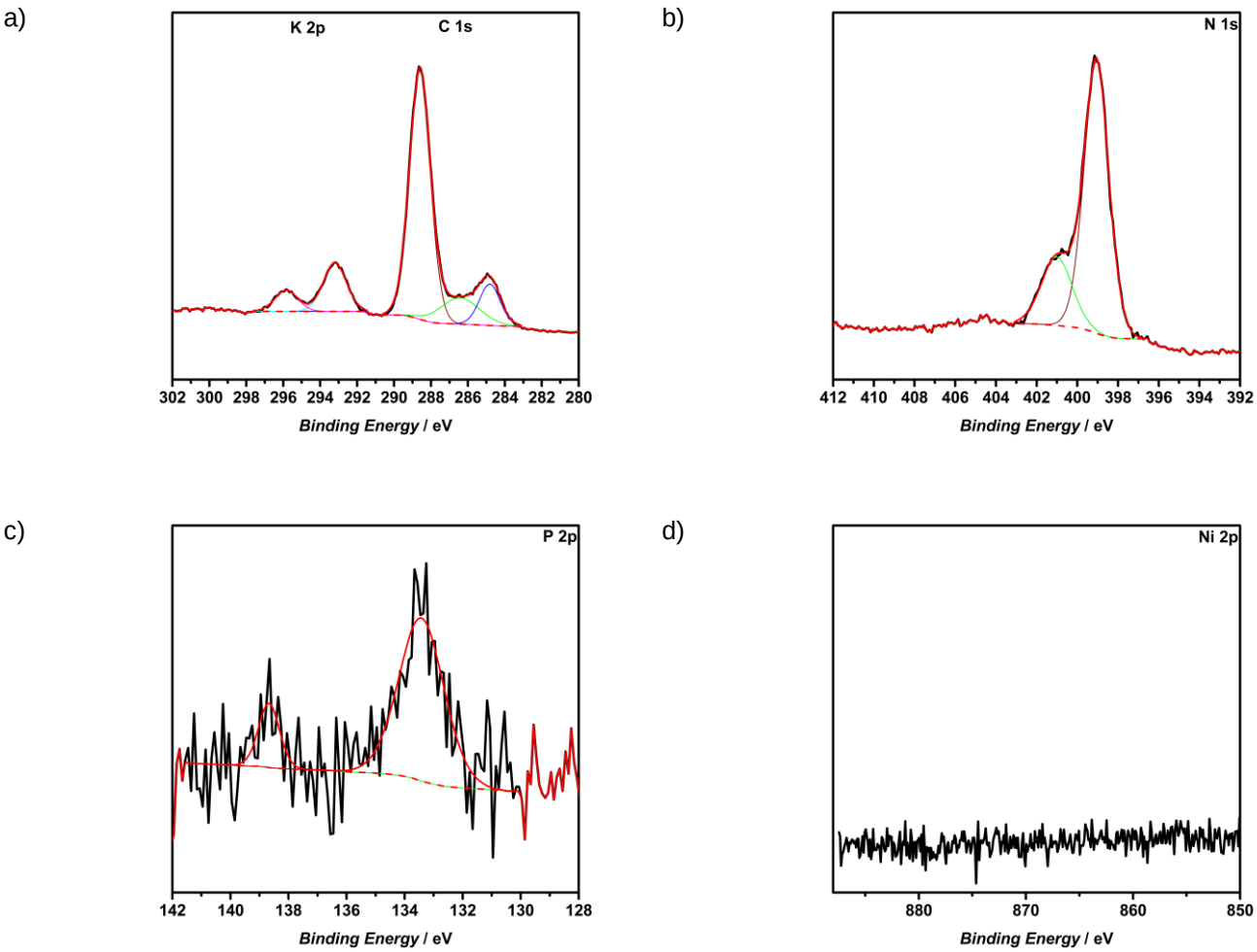

Figure S13. Characterization of $^{NCN}\mathbf{CN_x}$ after 24 hours of irradiation, in the presence of $^{NCN}\mathbf{CN_x}$ (5 mg), 4-MBA (30 μmol) and **NiP** (50 nmol) in KP_i (0.02 M, pH 4.5, 3 mL) solution (1 sun irradiation, AM 1.5G, 25°C), with XPS in the regions of a) K_{2p} and C_{1s}, b) N_{1s}, c) P_{2p} and d) Ni_{2p}. The K_{2p} and C_{1s} as well as N_{1s} spectrum are in good correlation with XPS results obtained from $^{NCN}\mathbf{CN_x}$ prior to photocatalysis. In the Ni_{2p} spectrum, there is no signal, indicating that most probably there is not any **NiP** catalyst physically adsorbed on the material surface after 24 hours of irradiation. The peaks in P_{2p} spectrum is likely to be due to phosphate buffer used during photocatalysis.

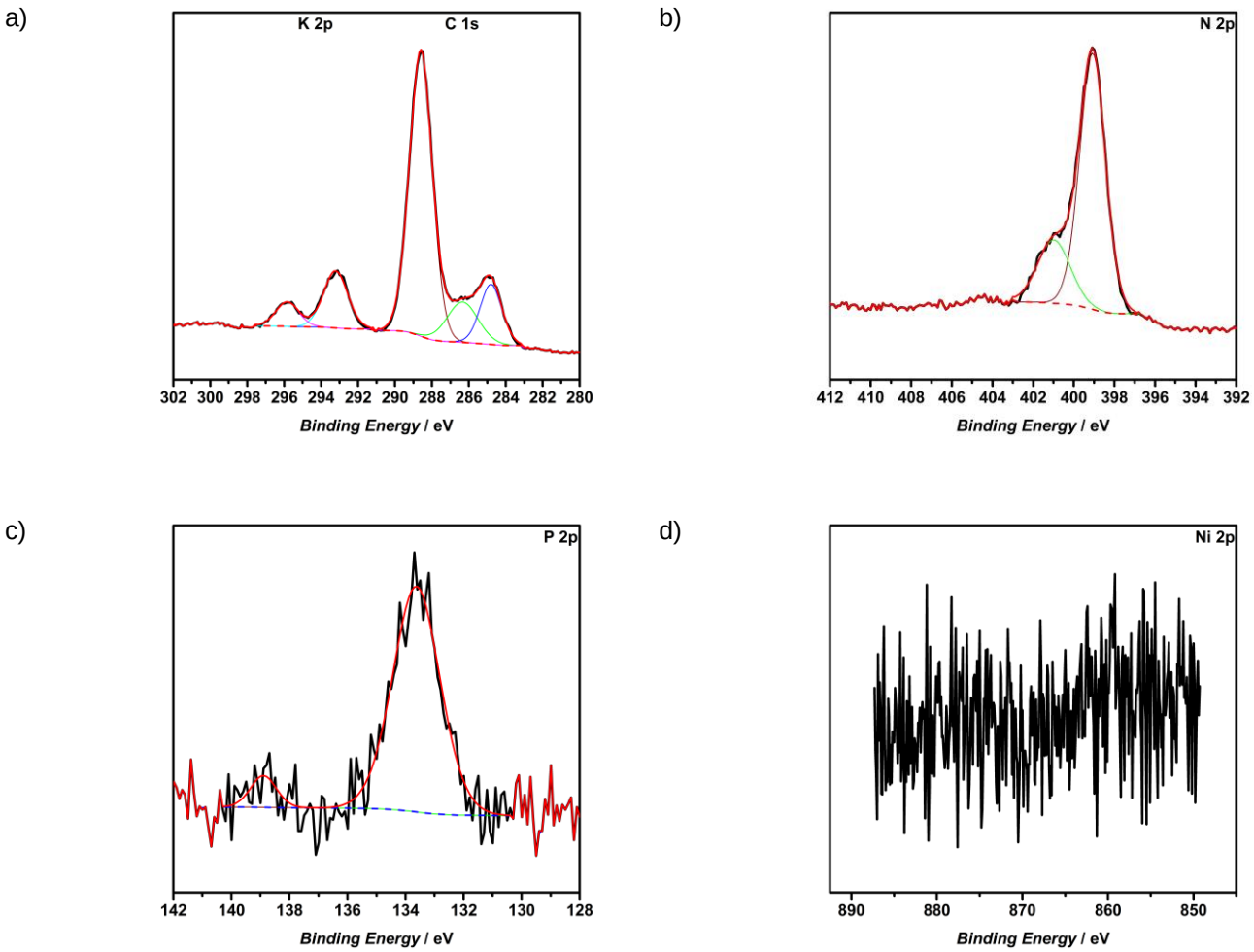

Figure S14. Characterization of $^{NCN}\mathbf{CN_x}$ 24 hours of irradiation, in the presence of $^{NCN}\mathbf{CN_x}$ (5 mg) and 4-MBA (30 µmol) in KP_i (0.02 M, pH 4.5, 3 mL) solution (1 sun irradiation, AM 1.5G, 25°C), with XPS in the regions of a) K_{2p} and C_{1s}, b) N_{1s}, c) P_{2p} and d) Ni_{2p}. The K_{2p} and C_{1s} as well as N_{1s} spectrum are in good correlation with XPS results obtained from pure $^{NCN}\mathbf{CN_x}$ prior to photocatalysis. The peaks in P_{2p} spectrum is likely to be due to phosphate buffer used during photocatalysis. As predicted, no peak in Ni_{2p} spectrum was detected as the photocatalysis was performed in the absence of **NiP**.

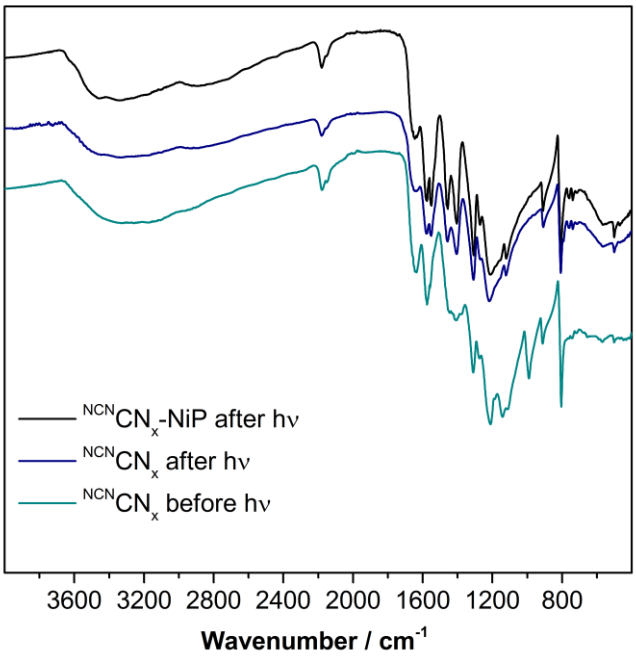

Figure S15. Comparing FTIR spectrum of ^{NCN}**CN$_x$** (5 mg) before irradiation and after irradiation (1 sun irradiation, AM 1.5G, 25°C) for 24 h in the presence of 4-MBA (30 μmol) in KP$_i$ (0.02 M, pH 4.5, 3mL) with and without **NiP** (50 nmol).

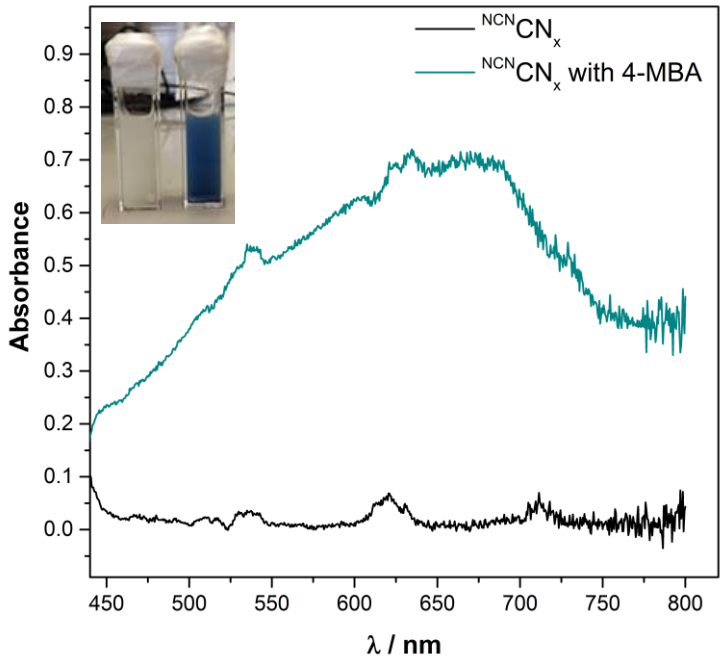

Figure S16. Colloidal suspensions of ^{NCN}**CN$_x$** (5 mg) in KP$_i$ (3 mL) and ^{NCN}**CN$_x$** (5 mg) and 4-MBA (30 μmol) in KP$_i$ (3 mL) were prepared. UV/vis spectra were recorded and the absorption spectra were generated by comparing samples before and after irradiation for 30 min (1 sun irradiation, AM 1.5G, 25°C). Inset: Solution of ^{NCN}**CN$_x$** (5 mg), and 4-MBA (30 μmol) in an aqueous KP$_i$ solution (0.02 M, pH 4.5) before irradiation (pale yellow) and after irradiation (blue).

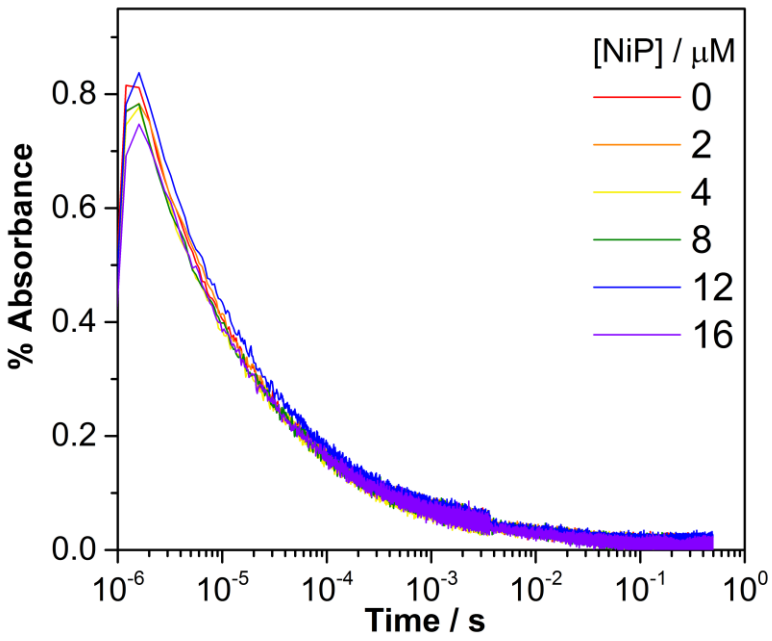

Figure S17. Transient decays probed at λ = 750 nm of $^{NCN}CN_x$ (5 mg mL^{-1}) suspension in aqueous KP_i solution (0.02 M, pH 4.5, 25°C) with varying concentrations of **NiP** following λ = 355 nm excitation.

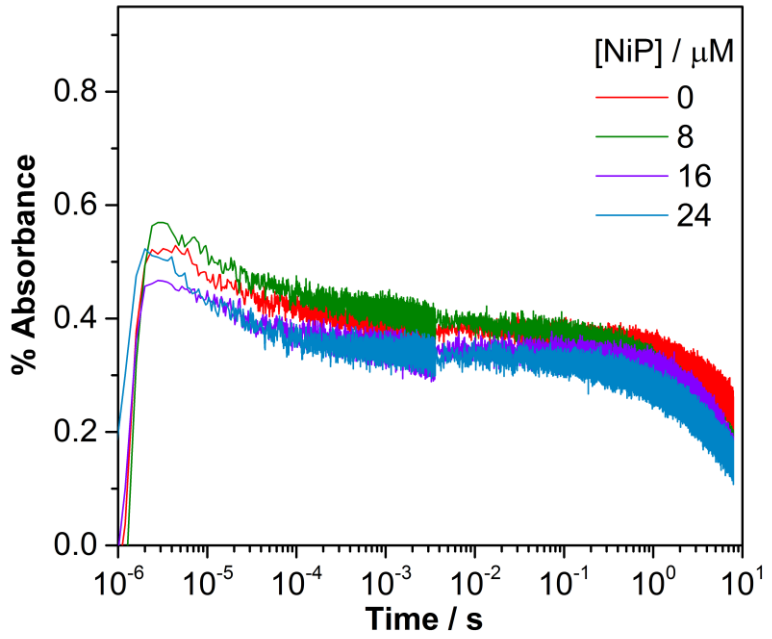

Figure S18. Transient decays probed at λ = 750 nm of $^{NCN}CN_x$ (1.2 mg mL^{-1}) suspension in aqueous KP_i solution (0.02 M, pH 4.5, 25°C) in the presence 4-MBA (10 mM) with varying concentrations of **NiP** following λ = 355 nm excitation. Note that changes in absorbance past ~ 2 s are caused by settling of the heterogeneous dispersion.

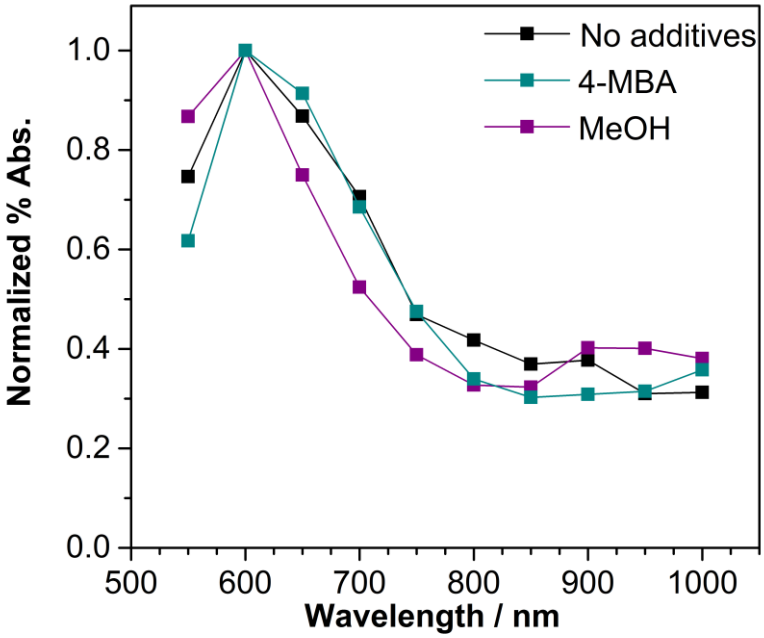

Figure S19. Normalized transient absorption spectra of $^{NCN}CN_x$ (1.2 or 5 mg mL^{-1}) suspension in aqueous KP_i solution (0.02 M, pH 4.5, 25°C, black line), spectra in the presence of 4-MBA (10 mM) and in a MeOH solution (20% by volume) following λ = 355 nm excitation are also shown. Spectra were taken at 100 µs delay time.

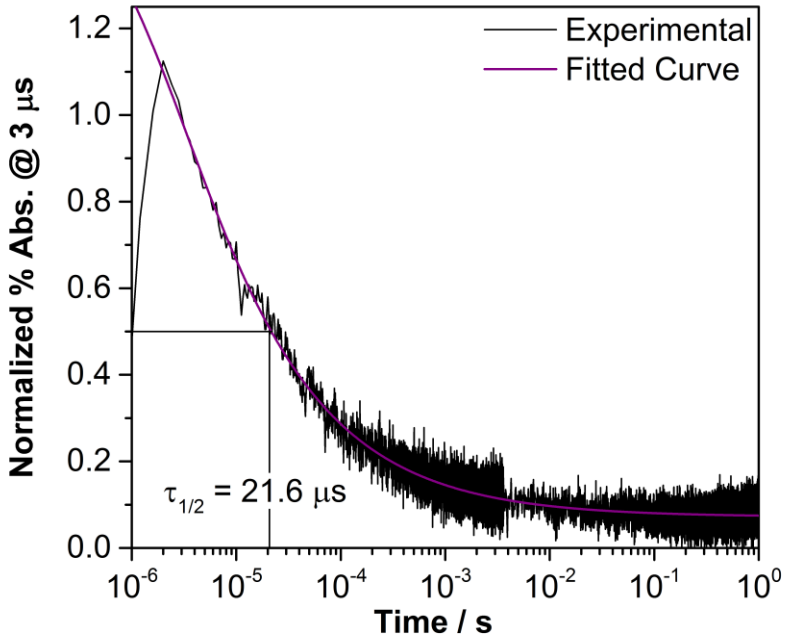

Figure S20. Normalized transient decay probed at λ = 750 nm of $^{NCN}CN_x$ (1.2 mg mL^{-1}) suspension in aqueous KP_i solution (0.02 M, pH 4.5, 25°C) following λ = 355 nm excitation. A power law fit (purple line) is overlaid to the experimental data (black line).

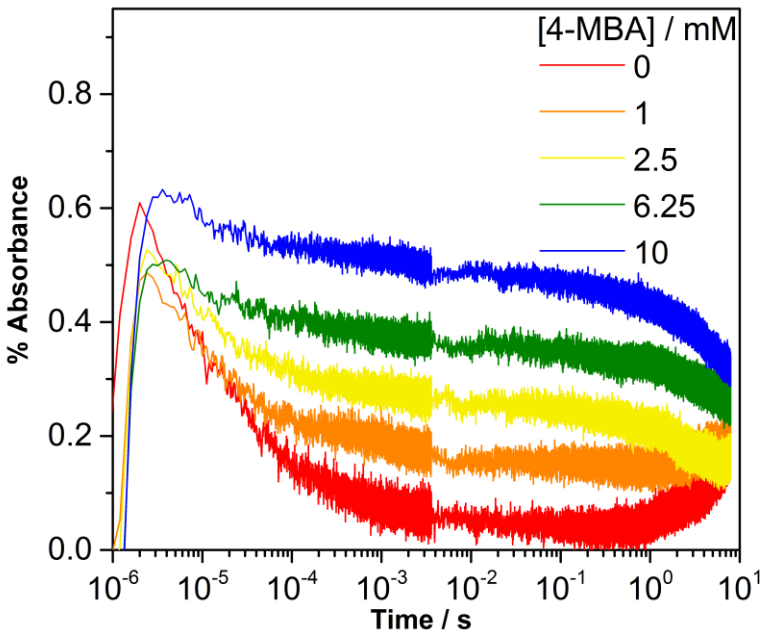

Figure S21. Transient decays probed at λ = 750 nm of $^{NCN}CN_x$ (1.2 mg mL^{-1}) suspension in aqueous KP_i solution (0.02 M, pH 4.5, 25°C) in the presence of varying concentrations of 4-MBA following λ = 355 nm excitation. Note that changes in absorbance past ~ 2 s are caused by settling of the heterogeneous dispersion.

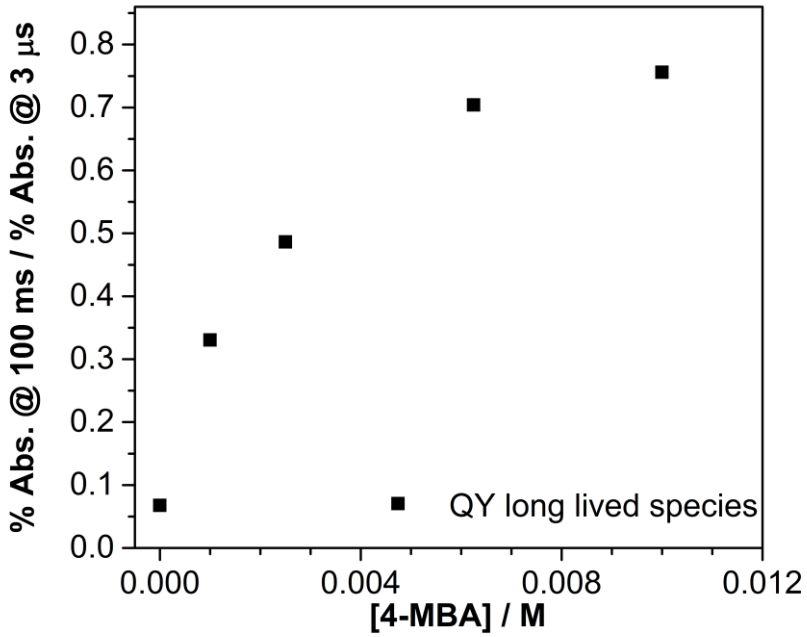

Figure S22. Yield of formation of the long-lived electron species versus 4-MBA concentration.

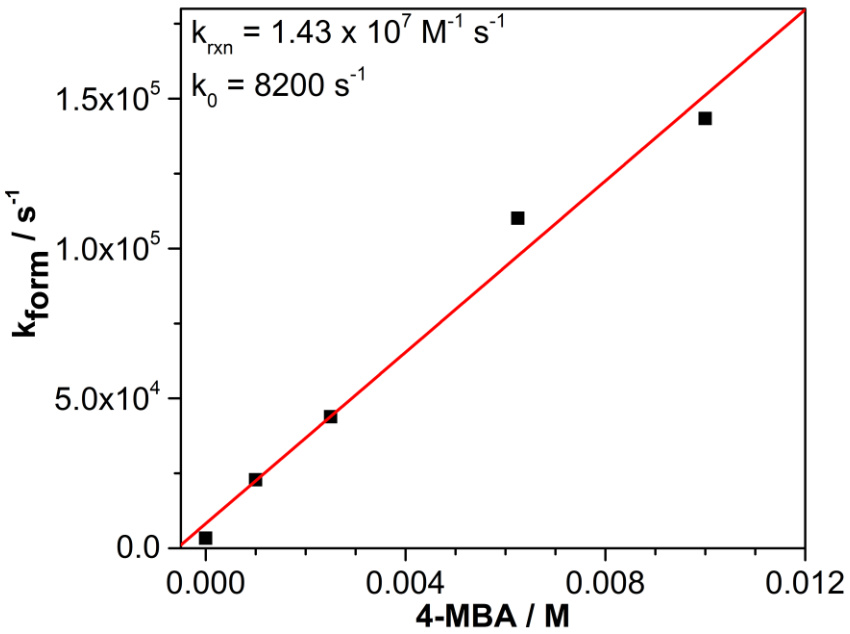

Figure S23. Rate of formation of the long-lived electron species versus 4-MBA concentration. The rate constant of reaction between ^{NCN}**CN$_x$** and 4-MBA is obtained from the slope of the linear fit, whereas the background rate is taken from the intercept.

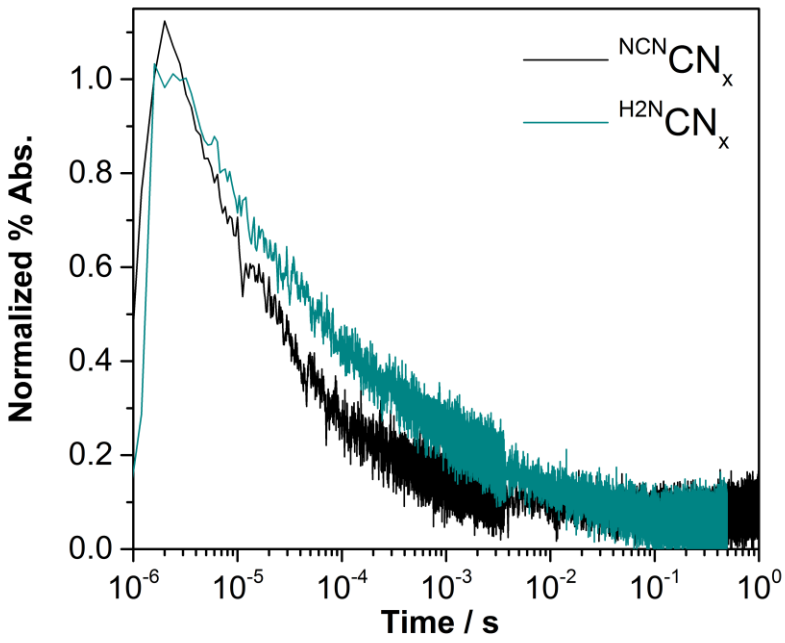

Figure S24. Normalized (at 3 µs) transient decays probed at λ = 750 nm of ^{NCN}**CN$_x$** (1.2 mg mL^{-1}) and ^{H2N}**CN$_x$** (1.2 mg mL^{-1}) suspensions in aqueous KP$_i$ solution (0.02 M, pH 4.5, 25°C) following λ = 355 nm excitation.

Supporting References

(1) Lau, V. W.-h; Moudrakovski, I.; Botari, T.; Weinburger, S.; Mesch, M. B.; Duppel, V.; Senker, J.; Blum, V.; Lotsch, B. V. *Nat. Commun.* **2016**, *accepted*, arXiv:1604.02131v1 [cond – mat.mtrl – sci].

(2) Thomas, A.; Fischer, A.; Goettmann, F.; Antonietti, M.; Müller, J.-O.; Schlögl, R.; Carlsson, J. M. *J. Mater. Chem.* **2008**, *18*, 4893–4908.

End of Supporting Information